JTTEE5 19:620–634
DOI: 10.1007/s11666-009-9454-7
1059-9630/$19.00 © ASM International

An Experimental and Finite Element Study of Cold Spray Copper Impact onto Two Aluminum Substrates

Peter C. King, Gyuyeol Bae, Saden H. Zahiri, Mahnaz Jahedi, and Changhee Lee

(Submitted June 18, 2009; in revised form September 3, 2009)

The effect of cold spray temperature and substrate hardness on particle deformation and adhesion has been studied, with particular emphasis on adiabatic shearing leading to melting. Copper particles were cold sprayed onto commercial purity (CP) aluminum and alloy 7050-T7451, with stagnation temperatures 200, 400, and 600 °C. Deposition efficiency, assisted by particle embedding, increased with temperature and was higher on the softer CP substrate. Crater surfaces, adhered particles, and interfaces were characterized by scanning electron microscopy, focused ion beam, and transmission electron microscopy. For comparison, the impact of 15 μm Cu particles was simulated using finite element modeling. A thin layer of material on the substrate-side of the interface was predicted to reach melting point on both substrates at higher impact velocities. Formation of a molten layer was found experimentally. At 600 °C, the effect of substrate heating by the gas jet could not be ignored.

Keywords bonding, cold gas dynamic spraying, finite element modeling, particle deformation

1. Introduction

1.1 Current Understanding of Cold Spray Bonding

As cold spray steadily gains popularity as a process for depositing layers of material in the solid state by the high-speed impact of microparticles, the question of under what conditions bonding occurs is becoming increasingly important (Ref 1). Two types of bonding can be identified: particle-onto-substrate, which is necessary for the formation of an initial monolayer of particles and which determines the adhesive strength of the final coating on the substrate; and particle-onto-particle, which allows a thicker deposit to build up, and ultimately influences the cohesive strength of the deposit. A particular advantage of cold spray is its capacity to bond together dissimilar materials. For example, metals with different crystal structures and even metallic coatings on ceramic or polymer substrate have been explored (Ref 2, 3). Also, common is the co-deposition of two or more materials, and here, as in the single-material case, cohesive bonding is critical (Ref 4). For continuing development of new applications, and the improvement of existing ones, more study is required to ascertain, at a sub-particle level, the nature of bonding in cold spray deposition.

Experimentally, it is known that there is a critical velocity for particle adhesion, v_c, which has a characteristic value for each different material, depending on its particular thermophysical properties. For instance, for copper impact onto copper, a v_c of 570 m/s has been measured (Ref 5). v_c can be influenced by feedstock purity and microstructure, and powder preheating. The choice of substrate material, when different to that of the particle, has been shown, both numerically and empirically, to also affect v_c (Ref 6, 7).

In the study of cold spray deformation mechanics, the problem is often reduced to that of a single, spherical particle impacting normally onto a flat surface. This is representative of the numerous impacts that are required to form a monolayer of one material onto another. The geometry has not only a high degree of symmetry, which lends itself to finite element modeling (FEM), but also allows ready comparison with experiment (splat studies) if spherical particles are used and the substrate is well polished. In splat studies, the substrate is exposed to limited numbers of impacts by using a low-powder feed rate, quick lateral movement of the nozzle past the substrate (or substrate past the nozzle), or with the aid of a mask (Ref 8). Isolated particles adhered to the surface may then be chosen for study. In practical application the substrate, depending on the chosen preparation technique and also the impact of other particles during spray, has a certain roughness, and the spray particles need not be spherical.

The supersonic impact of a cold spray microparticle onto a surface is characterized by deformation at very high strain rates (over 10^7 s^{-1}, Ref 9). The time from first contact to complete conversion of the particle kinetic energy to internal energy, or so-called "contact time," t_c, is typically less than 100 ns. Strain, far from being evenly

Peter C. King, Saden H. Zahiri, and **Mahnaz Jahedi**, CSIRO Materials Science and Engineering, Gate 5, Normanby Road, Clayton, VIC 3168, Australia; and **Gyuyeol Bae** and **Changhee Lee**, Kinetic Spray Coating Lab (NRL), Division of Materials Science and Engineering, Hanyang University, 17 Haengdang-Dong, Seongdong-Gu, Seoul 133-791, Republic of Korea. Contact e-mail: Peter.King@csiro.au.

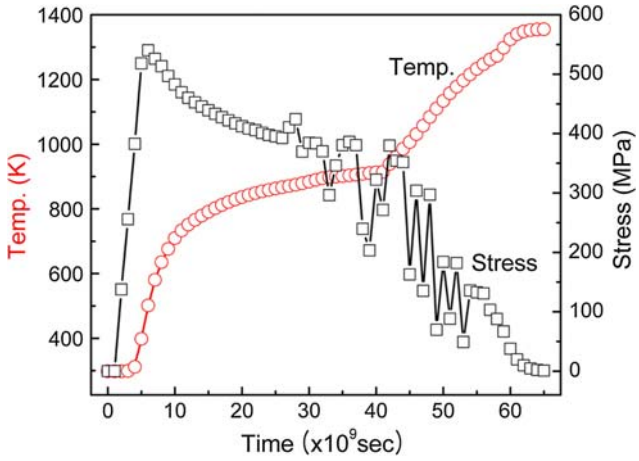

Fig. 1 Temperature and stress evolution within the interfacial jet of a 25 μm Cu particle during impact onto Cu (Ref 11)

distributed, is concentrated in the shear zones at the interface between particle and substrate, particularly at the peripheral regions of the particle. Heat evolved due to deformation results in thermal softening and in turn, further localization of deformation. Consequently, adiabatic shear instabilities develop at the interface. The material there behaves in a viscous-like manner, creating a fast, outward-moving "jet" of material, with strain rates in the order of 10^9 s^{-1} (Ref 10). Studies using the FEM technique agree on the following behavior. At a low-impact velocity (i.e., below v_c), strain, strain rate, and temperature at the particle-substrate interface increase monotonically with time over the entire contact period. However, for impact simulated above v_c (see Fig. 1) there is a further, sudden increase in each of these variables as the shear instability develops during the second-half of the contact period. Furthermore, there are large fluctuations in stress, as it drops to zero, the material losing shear strength. Interfacial temperatures approach, or reach melting point.

1.2 Interfacial Melting During Cold Spray Impact

The nature of bonding may be altered greatly if a small volume of molten material forms at the interface. However, there is some disagreement on the possibility of this occurring. Extensive modeling by Bae et al. (Ref 11) showed that in the impact of 25 μm particles at the critical velocity for each system, interfacial temperatures either reached the melting point or were very close. When dissimilar materials were chosen such that one was softer than the other, the softer component underwent greater deformation, with the formation of a liquid layer. On the other hand, Grujicic et al. (Ref 12) found that conditions for melting were only met over a small fraction of the interface, and that therefore melting does not play a key role in bonding. In another experimental and computational study (Ref 13), melting was not found in copper particle impact onto stainless steel, and it was concluded that the formation of a jetlike ejection at the edge of the crater was a requirement for bonding, but not melting.

Alkhimov et al. (Ref 14) applied a one-dimensional heat transfer model to the substrate/particle system, which assumed that heat released due to plastic work was concentrated within small zone of known thickness, adjacent to the interface. It was found that interfacial melting occurred above a critical particle size, which was a function of particle velocity, the initial particle and substrate temperatures, and thickness of the heat-release zone (e.g., 12 μm for Al-on-Al impact at 300 K).

In addition to theoretical and computational predictions, there exists a somewhat disparate body of experimental evidence of interfacial melting in cold spray. Table 1 attempts to summarize the results of a variety of studies published in the open literature. Cold-sprayed materials have ranged from those with low-melting points such as Sn and Zn (232 and 420 °C, respectively), to Ti, which melts at 1660 °C, well in excess of the temperatures used in cold spray. The gas stagnation temperature used in each study has been included in the table, since it is not possible to rule out heating due to impingement of the gas jet on the surface of the deposit during cold spray.

There are a variety of microstructural features that have been interpreted as evidence of melting, and which will be discussed individually here.

Most recognisable are ejecta from the impact events. They are typically in the form of submicron, spherical particles. Their diameters are smaller than those of the powder particles themselves (Ref 7). Material in the molten state reduces surface tension by assuming a spherical shape. However, long streaks or splashes are also possible (Ref 15). In splat studies, they emanate from craters or around adhered particles, usually thrown a short distance over the substrate surface. Spheroidized particles have also been observed on coating surfaces (Ref 16).

In the observation of empty impact craters, it is often possible to find signs of adhesive interaction between the substrate and rebounding particle. Wu et al. (Ref 17), for instance, showed small fragments of particle material, which remained on the surface of a mild steel substrate following impact by Al-12Si particles. They did not claim that this constituted evidence of fusion. However, similar features have been found in conjunction with other signs of melting, such as in the impact of aluminum particles onto a ceramic surface in Ref 7. Dimpled crater surfaces, showing ductile failure, are due to local softening of the surface layers of the substrate. Fracture surfaces of cold-sprayed deposits often exhibit these features (Ref 18), but on their own they do not necessarily imply melting.

In a number of studies, intermetallic phases have been found at the interface. Naturally, this is only possible when a combination of particle and substrate metals is chosen such that an intermetallic phase exists. It has been pointed out (Ref 19) that for intermetallic formation, the presence of liquid is necessary because solid-state diffusion, even at the melting point, is at least two orders of magnitude too slow to account for layer formation within $t_c < 100$ ns. Barradas et al. (Ref 19) found equiaxed intermetallic grains, 400 nm in size at cold spray copper-aluminum interfaces, while Guetta et al. (Ref 8, 20) observed intermetallic layers over 500 nm-thick. Wank et al. (Ref 21)

Table 1 Empirical evidence for interfacial melting during cold spray

Reference	Material system	Stagnation temperature, °C	Type of investigation	Evidence of melting
Barradas et al. (Ref 19)	Cu onto Al	550	TEM of coating-substrate interface	α_2-$AlCu_4$, η_2-AlCu, and θ-$CuAl_2$ phases found, in some places layers were 20 nm thick, in others, $CuAl_2$ grains were 400 nm in size
Bolesta et al. (Ref 22)	Al onto Ni	Not given	Grazing incidence XRD analysis of coating-substrate interface	Detection of Ni_3Al. Estimated interfacial layer thickness 20-50 nm
Guetta et al. (Ref 8, 20)	Cu onto Al	600	FIB/TEM study of single-particle interface with substrate	>500 nm-thick diffusion layer containing intermetallic phases θ-$CuAl_2$ and Cu_9Al_4. Also, Al-$CuAl_2$ eutectic region
King et al. (Ref 7)	Al onto PZT	350	Splat studies	Spheroidized particulate ejecta and signs of adhesive interaction
King et al. (Ref 7)	Cu onto Al	600	Splat studies	Spheroidized Al particulate ejecta
Li et al. (Ref 16)	Zn	320, 410	TEM of deposit cross section, SEM of deposit surface	Spheroidized particulates, recrystallised grains, amorphous regions
Li et al. (Ref 18)	Various; Al2319, Al12Si, Ti, Ti-6Al-4V, NiCoCrAlTaY	520-620	SEM observation of deposit fracture surfaces	Ductile failure, dimples
Ning et al. (Ref 15)	Al-10%Sn onto 304 stainless steel	~300	Splat studies	Ejecta
Vlcek et al. (Ref 53)	Ti-6Al-4V	Not given	SEM, TEM	Spheroidized particulates
Wank et al. (Ref 21)	Zn and Zn5Al onto Al 7022 and Mg AZ91	250	TEM studies of coating/substrate interface	Submicron and nanosized precipitates at interface: $MgZn_2$ and $Mg_5Zn_2Al_2$ and $Mg_{11}Zn_{11}Al_6$
Xiong et al. (Ref 26)	Al onto Al/Ni onto Al6061-T6	300, 400	TEM studies of interface	Formation of amorphous layer, 3 nm-thick
Zhang et al. (Ref 54)	Al onto Sn	Room temperature	SEM	Melting of substrate—details not given

referred to submicron-sized particles in their investigation of zinc-based coatings onto aluminum- and magnesium-alloy substrates. Using a sensitive synchrotron XRD technique, Bolesta et al. (Ref 22) detected a 20-50 nm Ni_3Al layer beneath a cold spray aluminum coating on a nickel substrate.

Signs of fluid-like behavior at the interface have been noted, manifest in the sort of wavy interfaces that are also found in explosive welding due to Kelvin-Helmholtz instability (Ref 23). Thus in cold spray, interfacial waves and ripple effects (Ref 19, 24, 25) roll-ups and vortices (Ref 21) have been reported on a micron-scale. While fluid-like flow can occur without melting, it has been commonly found in conjunction with the appearance of intermetallics, and may assist the latter through turbulent mixing of the two metals (Ref 21).

In other work, a 3-nm amorphous layer was found at the interface (Ref 26). It was proposed that it had formed by rapid quenching from the melt, and perhaps stabilized by alloying due to diffusion across the interface. Guetta et al. (Ref 20) observed an amorphous Al-O phase at the interface between a copper particle and aluminum substrate. Similarly, a partially amorphous layer consisting of a mixture of iron and titanium oxides has also been found at the interface between a titanium particle and steel substrate (Ref 27). There was no mention of how the oxide layers compared with those existing on the surfaces before spray.

1.3 Current Investigation

In this study, a combined computational/empirical approach is applied to the problem of bonding at copper-aluminum interfaces. FEM provided an estimation of the at-rest morphologies of the deformed particle and substrate, and the temperatures evolved at the interface. While this assisted interpretation of the experimental data, the latter provided validation of the accuracy of the model.

Three different experimental approaches were taken:

- A quantitative analysis of the fraction of adhered particles, which included the effect of different variables; spray temperature and substrate.
- Characterization of the failure surface formed due to brief contact between the impacting and rebounding particle with the substrate. Signs of melting and adhesive interaction were of particular interest.
- Cross-sectional investigation of deformed particles and the particle-substrate interface by focused ion beam/secondary electron microscopy (FIB/SEM) and transmission electron microscopy (TEM).

2. Experimental Methods

In order to investigate the effect of substrate properties, particularly hardness, on bonding, copper particles were sprayed onto two different aluminum alloys; a commercial purity (CP) aluminum and alloy 7050-T7451

(Al-5.75Zn-2.06Mg-2.06Cu-0.08Fe-0.05Si-0.12Zr). The 7050 alloy was chosen for its high strength in comparison with CP aluminum, the homogeneity of its microstructure and low concentration of intermetallic particles. The fine substrate microstructure minimized variation in the deformation and bonding behavior of the copper particles with impact location. Both substrates were prepared prior to cold spray by polishing with 1 μm diamond suspension, and cleaning with ethanol. The copper powder had an approximately spherical morphology. Laser particle size analysis using a Malvern Mastersizer X, showed that the average particle diameter (d_{50}) was 15.2 μm, with 10% of particles below $d_{10} = 9.8$ μm and 10% above $d_{90} = 22.7$ μm (Ref 7). A CGT Kinetiks® 3000 cold spray system was used with N_2 accelerant gas and an upstream pressure of 25 bar to spray Cu particles onto the substrates, at a standoff distance of 20 mm and traverse speed 0.05 m/s.

Three stagnation temperatures were chosen; $T_0 = 200$, 400, and 600 °C. The amount of substrate heating due to impingement of the gas jet was measured using an Agema Thermovision 570 Infrared Camera. The camera had a 320 × 240 pixel uncooled microbolometer with a spectral range of 7.5-13 μm and measurement accuracy of ±2%. It was equipped with a 24° × 18° lens. Images were analysed using the Irwin Research 2.01 software package. CP aluminum material was used with the surface ground using 120-grit SiC paper to reduce reflectivity and create a constant, reproducible emissivity, which was measured to be 0.43.

The effect of T_0 on particle velocity is shown in the right-hand column of Table 2, which gives the velocity, v_e, of a 15-μm copper particle at the nozzle exit. Particle velocity was calculated using a one-dimensional isentropic model. This method has been commonly used to predict particle velocities in cold spray (Ref 28-30) so will be only briefly explained here. It has shown to give a good approximation to values measured experimentally (Ref 31). Particle travel is along the nozzle axis, and gas flow there is assumed to be unaffected by the boundary layer at the nozzle wall. According to isentropic theory, the Mach number, M, can be determined at any location in a shock-free, supersonic nozzle from the ratio of nozzle area at that point, A, to the throat area A^*, as per the area-Mach relation (Eq 1) (Ref 32).

$$\left(\frac{A}{A^*}\right)^2 = \frac{1}{M^2}\left[\frac{2}{\gamma+1}\left(1+\frac{\gamma-1}{2}M^2\right)\right]^{(\gamma+1)/(\gamma-1)}, \qquad \text{(Eq 1)}$$

where γ is the specific heat ratio.

Table 2 Cold spray experimental plan

Experiment no.	Stagnation temperature, °C	Substrate	15 μm particle v_e (calculated), m/s
1	600	CP Al	6.6×10^2
2	600	Al 7050	6.6×10^2
3	400	CP Al	6.2×10^2
4	400	Al 7050	6.2×10^2
5	200	CP Al	5.5×10^2
6	200	Al 7050	5.5×10^2

Other local properties of the gas phase—temperature, pressure, density, and velocity—are simple functions of M, γ, and the stagnation conditions (Ref 32). The dependence of viscosity on local temperature was determined using Sutherland's formula (Ref 33).

For a spherical particle of diameter d_0 and density ρ_p, particle acceleration was calculated according to Eq 2, which is derived from Newton's second law and the expression for drag force on the particle (Ref 28).

$$\frac{dv_p}{dt} = \frac{3C_D\rho_g}{4d_0\rho_p}(v_g - v_p)^2, \qquad \text{(Eq 2)}$$

where v_p is the particle velocity, ρ_g and v_g are the gas density and velocity, respectively, and C_D is the drag coefficient. C_D was calculated according to the correlations derived by Henderson (Ref 34).

Using a time step of 5×10^{-6} s during the early stages of particle acceleration ($v_p < 80$ m/s) and 3×10^{-7} s thereafter, the gas conditions at the current particle location were calculated, then Δv_p was obtained from Eq 2, followed by the new particle location for the next time interval. This process was repeated until the particle reached the nozzle exit.

In practice, particles moving along a trajectory away from the nozzle axis tend to experience less acceleration. The precise effect of angular trajectory on velocity could not be determined without higher-dimensional modeling of the flow field. Observation of the bonded particles revealed that a significant proportion appeared to have impacted at an angle not exactly perpendicular to the surface. Furthermore, isentropic theory does not allow any consideration of the behavior of the particles outside the domain of the nozzle, and in the free jet there may be some additional acceleration, followed by deceleration of the particles through the bow shock at the substrate surface. Thus, the velocity of particle impingement onto the substrate, v_i, is not equal to v_e. Computational fluid dynamic (CFD) modeling of cold spray of copper (Ref 35) has shown that particle acceleration in the free jet is generally small compared with that inside the nozzle, while the effect of bow shock deceleration is only noticeable for the smallest, micron-sized particles (i.e., those with the lowest inertia). Most importantly, while modeling yields a single value of v_i for a given particle size, d_0, in the experimental observation of individual sprayed particles some variation in-flight behavior must be borne in mind.

Thick coatings (>3 mm) were produced using all of the experimental conditions (nos. 1-6) listed in Table 2. Each sample was then cross-sectioned, and the coating-substrate interface investigated by optical microscopy (OM).

For splat studies, experiments 1-6 in Table 2 were performed again, but this time, a reduced powder feed rate was used, and the nozzle was moved past the substrate in a single swipe so that only a limited number of particles were deposited. Each sample surface was then examined using an xT Nova NanoLab 200 dual beam FIB/SEM. The FIB/SEM instrument included a field emission source and in-lens SE detector for high-resolution imaging

and an EDX system. Isolated impacts could be observed, and in the case of two samples sprayed at 600 °C (nos. 1 and 2), rectangular trenches were milled into the embedded Cu particles using the Ga^+ beam, to produce cross sections. The morphology and internal microstructure of the particles and surrounding substrate were then examined in situ. The depth of penetration was compared with that predicted under similar impact conditions by FEM.

A foil for TEM of the Cu-CP Al interface was prepared in the FIB/SEM. The H-bar technique was employed, which has been described in detail elsewhere (Ref 36, 37). TEM was performed using a Philips CM30 operating with a LaB_6 electron source at 200 kV and an FEI Tecnai™ G^2 F20, with a field emission source at 200 kV.

Particle impacts were simulated by a nonlinear, transient finite element model using the commercial finite-element package, ABAQUS 6.7-2. Since the particle bonding process involves short dynamic response times and large deformations, the explicit time integration algorithm (Ref 38) was chosen. A fully coupled thermal-stress analysis was performed to obtain an accurate thermomechanical response under high strain rate deformation conditions. Figure 2 shows the FE model constructed for the present work. Four-node bilinear axi-symmetric quadrilateral mesh elements with reduced integration and hourglass control (CAX4R) from the ABAQUS element library were used, and a surface-to-surface penalty contact algorithm with balanced contact pair formulation (Ref 38) was applied between particle and substrate. Refinement of the mesh at the impacting interfaces was subsequently performed for more accurate computations. Arbitrary Lagrangian-Eulerian (ALE) adaptive remeshing (Ref 38) was also performed to avoid mathematical truncation errors due to severely distorted elements.

The Johnson-Cook plasticity model (Ref 39), given by Eq 3, was employed to describe the rate and temperature dependence of material behavior during plastic deformation. The equivalent flow stress, σ, is expressed as:

$$\sigma = \left[A + B\varepsilon_p^n\right]\left[1 + C\ln\left(\frac{\dot{\varepsilon}_p}{\dot{\varepsilon}_0}\right)\right][1 - (T^*)^m], \qquad \text{(Eq 3)}$$

where ε_p and $\dot{\varepsilon}_p$ are the equivalent plastic strain and strain rate, respectively, and $\dot{\varepsilon}_0$ is the normalizing reference strain rate. Parameters A, B, C, n, and m are material-specific parameters; A is the yield stress, B and n represent the effects of strain hardening, C is the effect of strain-rate hardening, and m is a thermal-softening term. T^* is the homologous temperature.

The Johnson-Cook parameters and other physical properties for the materials used in the simulations are given in Table 3. The data in Table 3 were taken from material databases and the literature (Ref 39-41). Alloys 1100 and 7075 were chosen as the closest available approximation to the CP aluminum and alloy 7050 used in the experiments, respectively. Then, 15 μm copper particles were simulated in normal impact onto two aluminum alloy substrates at velocities $v_i = 310$, 430, 550, 670, and 890 m/s.

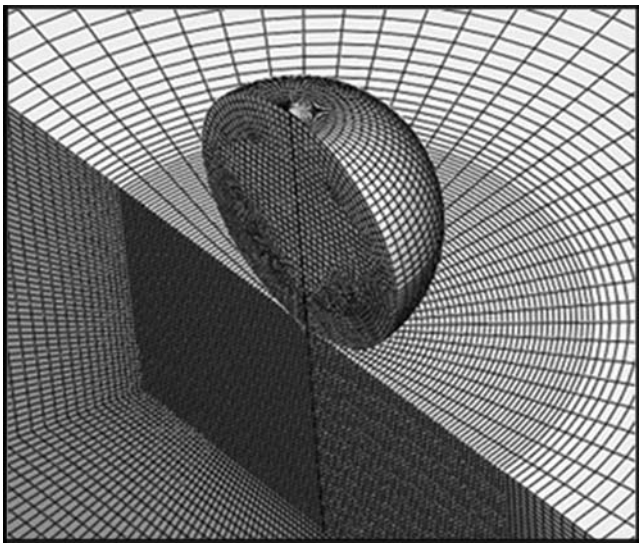

Fig. 2 Finite element model for particle/substrate impact simulation (Ref 11)

3. Results

3.1 Bulk Coating: Substrate Interfaces

Optical cross sections of the coating-substrate interfaces are shown in Fig. 3. In all cases, there was considerable roughening of the substrate due to embedment of the copper particles below the surface. The depth of penetration was dependent on particle size and velocity, which were subject to variation even at a constant gun temperature and pressure. Aluminum, trapped between neighboring impacts, was extruded upward, between the particles. Extensive plastic flow of the aluminum was noticeable on both substrates, regardless of spray temperature. However, total encapsulation of some particles due to their deep subsurface penetration was only seen on the softer, CP aluminum. Differences in the interfacial profile due to increasing the stagnation temperature from 200 to 600 °C were not as large as expected, despite the significantly deeper particle penetration (which will be

Table 3 Material properties used in the FE model

Material	Cu	Al 1100-H12	Al 7075-T6
Density, kg m^{-3}	8960	2710	2810
Young's modulus, GPa	124	68.9	71.7
Poison's ratio	0.34	0.33	0.33
Heat capacity, J kg^{-1} K^{-1}	383	904	960
Melting temperature, K	1356	916	908
A, MPa	90.0	148.4	496.0
B, MPa	292.0	345.5	310.0
n	0.310	0.183	0.3
C	0.025	0.001	0
m	1.09	0.895	1.2
Reference temperature, K	298	293	298
Reference strain rate, s^{-1}	1	1	1

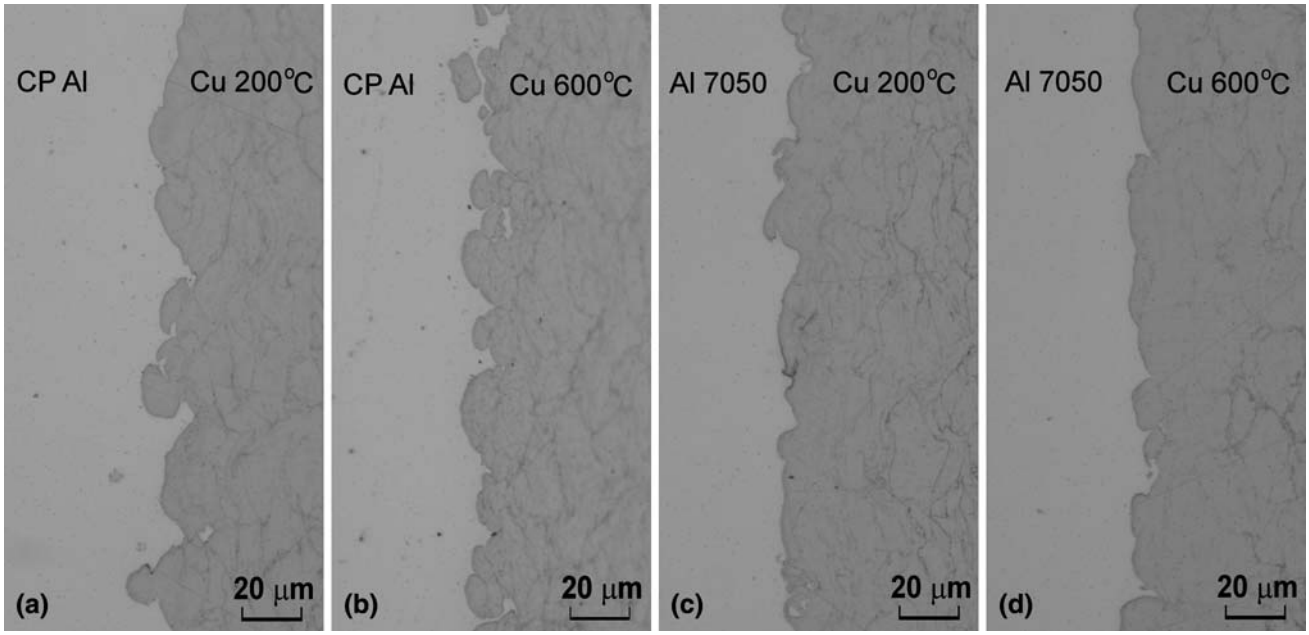

Fig. 3 Optical micrographs of coating/substrate interfaces. (a, b) CP aluminum substrate, (c, d) 7050 substrate, (a, c) $T_0 = 200$ °C, and (b, d) $T_0 = 600$ °C

demonstrated in the single-particle investigations, Section 3.3). This may have been due to the lower deposition efficiencies at $T_0 = 200$ °C, which resulted in a greater number of particle impacts directly onto the substrate surface before a completely covering monolayer was formed. With more impacts, further substrate deformation and roughening occurred, compensating to some degree for the reduced subsurface penetration per particle.

3.2 Particle Bonding Ratios

SEM examination of the surfaces following brief exposure to the cold spray particle and gas jet showed that under spray conditions producing low v_e ($T_0 = 200$ °C), few particles adhered successfully to the substrate. Most tended to rebound, leaving behind empty craters. At $T_0 = 600$ °C, v_e increased according to Table 2, and adhered particles then far outnumbered craters. The deposition efficiency, defined as the fraction of total impacts (adhered particles + craters) that resulted in adhesion, was plotted as a function of spray temperature and substrate type (Fig. 4). Each result was an average of measurements taken from several micrographs, each micrograph containing, on average, ~80 copper particle impacts. Error bars in Fig. 4 represent standard deviation. It was found that deposition efficiency increased with spray temperature, and was higher on the softer CP substrate. The transition from the erosive (rebound) to the deposition regime shifted to lower velocities on CP aluminum.

3.3 FEM Modeling and Deformation Behavior

Figure 5 shows cross-sectional views of the modeled particle/substrate systems at two different impact velocities.

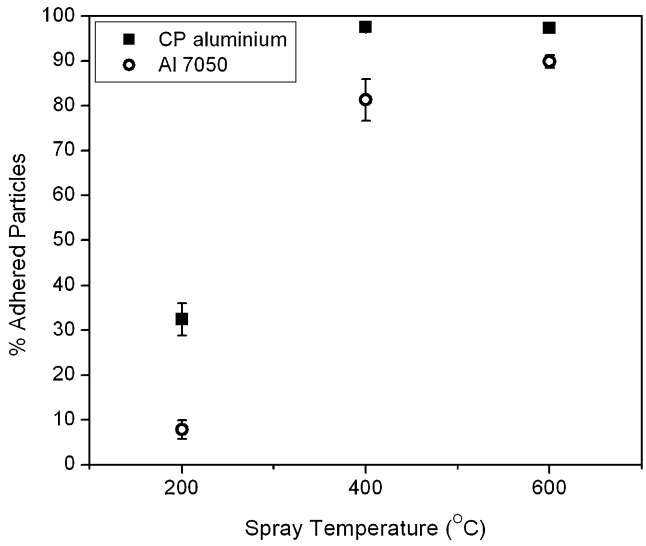

Fig. 4 Adhered copper particles, as a percentage of total copper impacts (adhered particles + empty craters)

There was greater subsurface penetration as v_i was increased, and greater penetration into the softer Al-1100 substrate compared with the 7075 alloy. Figure 5 can be compared with the embedded copper particles, sprayed at 600 °C (Fig. 6). Dissections performed in the FIB/SEM (Fig. 6c, d) revealed a deformed shape which closely resembled the simulations at higher v_i.

With large penetration depths, the exposed sections of the crater walls were deep and near-vertical. Modeling showed that, at sufficiently high velocities, the particles could become trapped within their own craters due to flattening and expansion of the particles perpendicular to

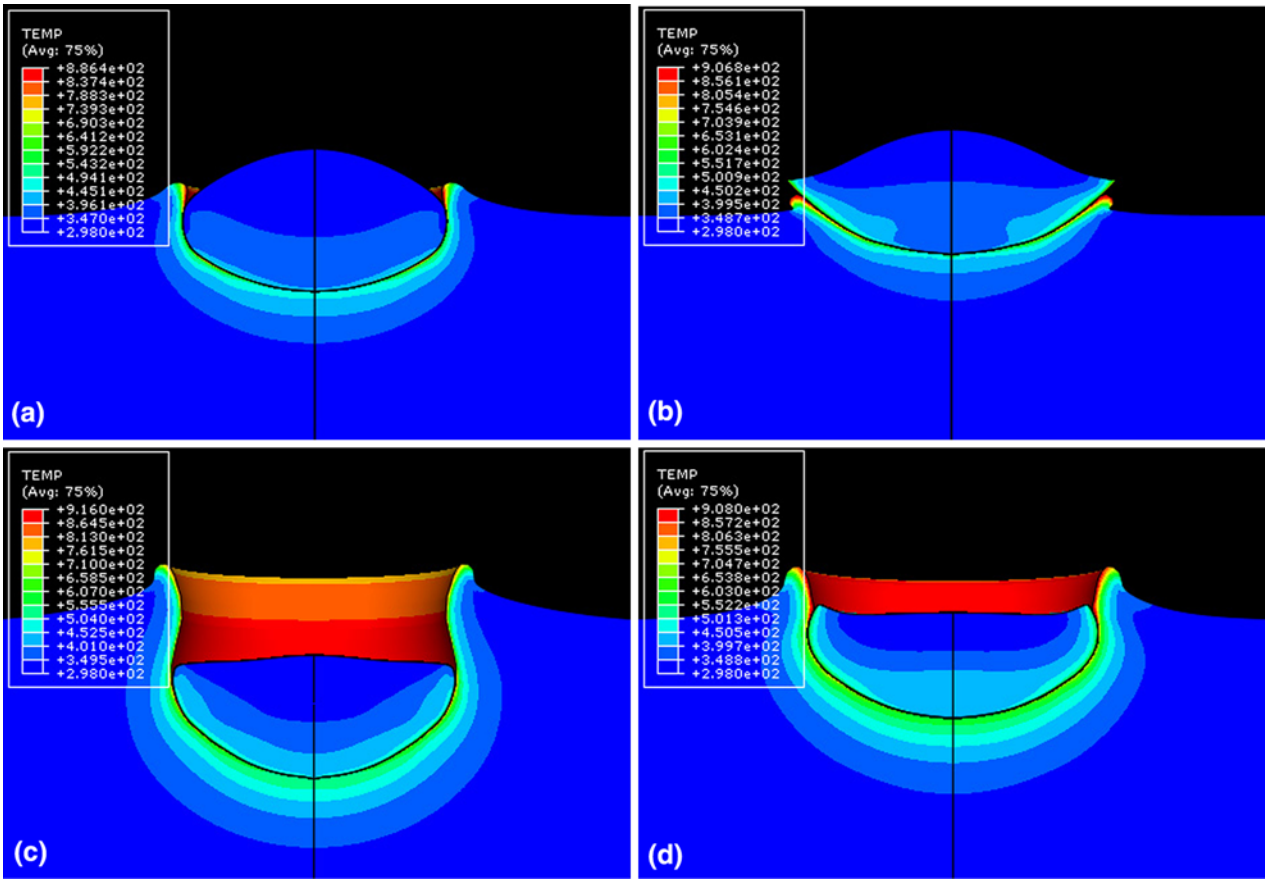

Fig. 5 Cross-sectional morphology and temperature distribution of deformed particle/substrate systems; (a) Cu-Al1100, $v_i = 430$ m/s, (b) Cu-Al7075, $v_i = 430$ m/s, (c) Cu-Al1100, $v_i = 670$ m/s, and (d) Cu-Al7075, $v_i = 670$ m/s

the impact direction, and constriction of the crater opening itself. This was possible with v_i as low as 430 m/s on the 1100 substrate, or at 670 m/s on the 7075 substrate. In the experiments, loss of contact between the particle and substrate was sometimes seen in places along the interface. Figure 6(d) is an example of a particle that seemed to have become almost completely detached from the substrate.

The penetration depth, P of an impacting particle is usually defined as the vertical distance from the base of the particle to the undeformed substrate surface (Ref 42, 43). Figure 7(a) uses the dimensionless ratio P/d_0, where d_0 is the initial particle diameter, to compare penetration depths from the FEM and FIB investigations. In the splat investigations d_0 was not known directly, but could be calculated from the volume of the deformed particle, V. V was determined from the cross section by assuming rotational symmetry about the particle vertical axis, taking n measurements of the particle diameter, d_i at regular intervals, Δh_i down the particle, then calculating the Riemann sum:

$$V = \sum_{i=1}^{n} \frac{\pi d_i^2}{4} \Delta h_i. \qquad \text{(Eq 4)}$$

Assuming an initially spherical particle, d_0 was obtained from Eq 5:

$$d_0 = \sqrt[3]{\frac{6V}{\pi}}. \qquad \text{(Eq 5)}$$

For this kind of quantitative analysis, a particular advantage of the FIB technique over standard mechanical polishing was that the exact bisection of the particle could be obtained. It was seen that FEM modeling tended to underestimate the penetration depths determined empirically. However in the model, the initial particle and substrate temperatures were set to 298 K. In practice, a high temperature region forms in the gas jet in front of the substrate due to the bow shock effect (Ref 44). The surface temperature rise on the CP aluminum substrate during a single pass of the nozzle, with the powder feed turned off and the substrate initially at ambient temperature, was measured to be 413 ± 1 K. With multiple passes of the gun, it was possible to achieve higher substrate temperatures. By holding the nozzle over the substrate for ~1 min, the temperature stabilized at 653 ± 3 K. However, in the splat investigations, only single passes were used. Therefore, to investigate the effect of gas-substrate heating, a simulation of the 670 m/s impact onto

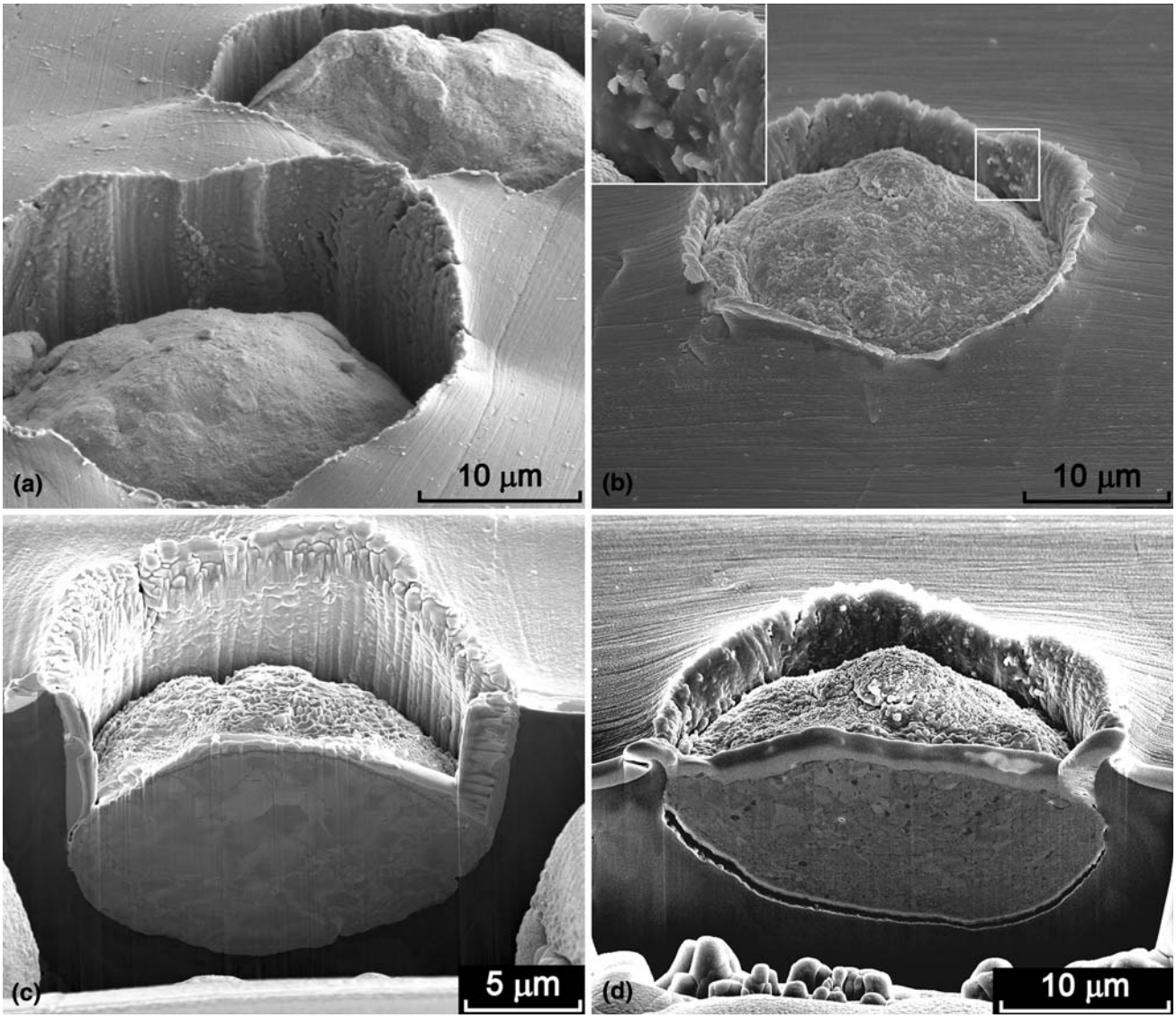

Fig. 6 Surface imaging (a, b) and FIB dissections (c, d) of copper particles embedded in the (a, c) CP Al and (b, d) Al 7050 surfaces; (a) Cu-CP Al, $T_0 = 600$ °C, (b) Cu-Al 7050, $T_0 = 600$ °C, (c) Cu-CP Al, $T_0 = 600$ °C, and (d) Cu-Al7050, $T_0 = 600$ °C

CP Al was run with the substrate initially at 413 K. The particle temperature was left at 298 K, since heat transfer from the gas phase to the particles was neglected. This may be not be completely unjustified, since any heating of the particles that occurs within the converging section of the nozzle is partly reversed past the throat, because the gas stream cools greatly as it expands. However, work is in progress to measure the temperature of the in-flight particle stream, and future modeling may incorporate these data as well.

The result of the 413 K simulation is shown in Fig. 7(a), and this point was found to lie much closer to the empirical data. This indicated that substrate softening could explain the deeper penetrations that were observed.

Figure 7(b) shows that the contact time, for all simulations was below 50 ns, but was generally higher on Al 1100 due to deeper penetration into this material.

The temperature distribution within the particle and substrate due to adiabatic deformation was also examined (Fig. 5). Due to localization of deformation, the temperature rise throughout most of the particle and substrate was small, except for a thin layer of material either side of the interface. In the 670 m/s impact of copper onto aluminum 1100 at room temperature, saturation at the melting point of aluminum 1100 (916 K) was achieved within a layer of the substrate, which was 55 nm at its thickest. With the substrate preheated to 413 K, an 85 nm-thick layer resulted. The physical extent of melting point zone is best seen in Fig. 8 and 9. Note that, in neglecting heat transfer, the model allowed for a temperature discontinuity across the interface. Thus, it was found that the substrate-side temperatures were always greater than those on the particle-side. Previous work (Ref 11) has shown that even when identical substrate/particle

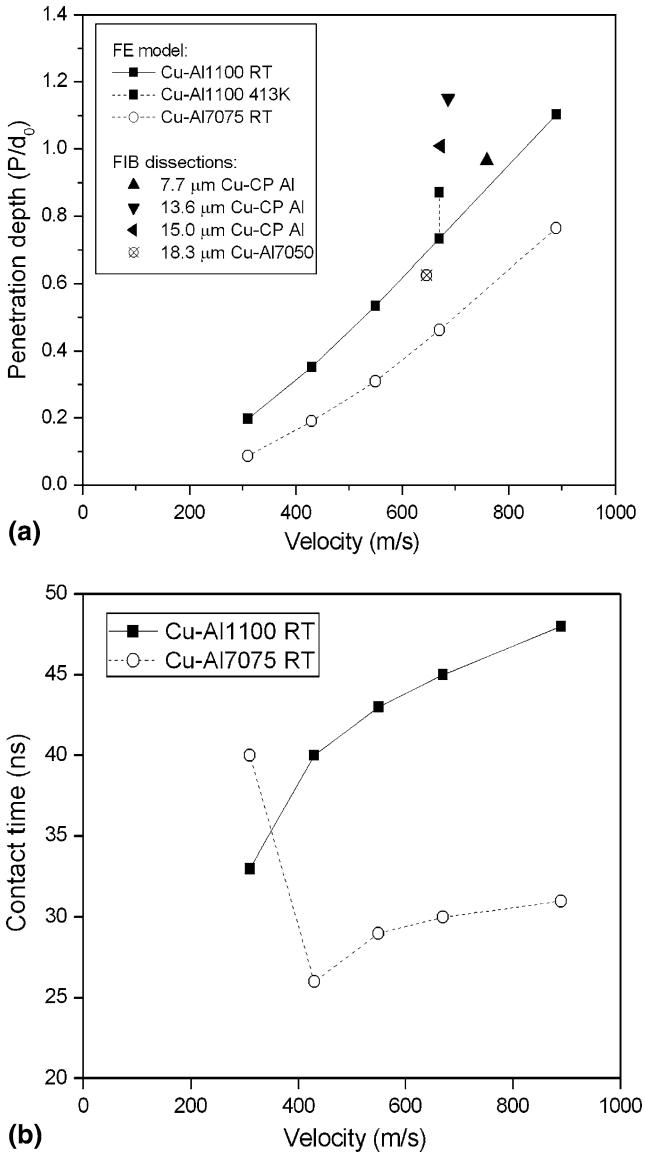

Fig. 7 (a) Normalized penetration depth—comparison of FEM and empirical data and (b) contact time according to FEM simulations

materials are considered, higher temperatures are reached on the substrate side of the interface. However, the discrepancy becomes greater still when dissimilar materials are involved.

The highest interfacial temperatures were found at or near the edge of the craters. On the softer Al 1100 substrate, the melting temperature (916 K) was achieved at 670 m/s and above. With further increase in velocity, the substrate melting point region spread over a larger area of the interface. Since a large share of kinetic energy was expended by deformation of the soft substrate, particle deformation was limited, particularly at low velocities. However, with increasing impact velocity, interfacial temperatures on the particle-side also rose.

Against the harder substrate, the particle-substrate interaction was rather different. Figure 8(b) shows that a large proportion of the crater surface had almost reached melting point (908 K) by 430 m/s. This was due to the harder alloy's greater tendency to strain localization (craters were shallower, but with more intensive deformation just below the particle). As with Cu-Al 1100, the melting point region occupied a larger fraction of the interface as v_i was increased. With resistance from the substrate, the particle underwent greater deformation and jetting was evident. Higher interfacial temperatures also developed on the copper side, but not to the point of melting.

At the lowest impact velocity, 310 m/s, on the 7075 alloy, the effect of strain hardening of the substrate became dominant over thermal softening. The impact mode could no longer be described as penetrative as energy dissipation was more evenly shared by particle and substrate. An anomalous increase in contact time resulted (Fig. 7b). No such transition was found in the Cu-Al 1100 system, as penetration depth and contact time increased monotonically with v_i, due to a steadily increasing dissipation of particle impact energy by substrate deformation.

3.4 Craters and Surface Investigation

Upon examination of the surfaces of both substrates following bombardment by copper particles, signs of melting were found under all conditions, 200-600 °C. Ejecta radiated outward from the craters over the surface of the substrate (Fig. 10). They were numerous at 600 °C, less frequent at 400 °C, and only occasionally observed at 200 °C. Note that Fig. 10 shows ejecta at $T_0 = 200$ °C. EDX spectra were collected using a finely focused spot at 5 kV (the Al K_α and Cu L_α peaks both lie below 2 keV). A survey of the CP Al surface sprayed at 600 °C showed that the ratio of Cu at.% to Al at.% was <0.05. Since the copper signal was so low compared to the aluminum, and may have been only a result of background effects, it is reasonable to assert that the ejecta had been caused entirely by melting of the substrate at the crater lip.

At $T_0 = 200$ °C craters on the CP aluminum substrate were shallow, bowl-shaped depressions, that did not give much indication of localized deformation. On the crater floors at least two morphologies could be distinguished; areas with uni-directional grooves (Fig. 11b), and dimpled areas (Fig. 11c). The dimpled surfaces were caused by thermal softening of the substrate just prior to detachment of the particle. Grooves were usually found at the edges of the crater and indicated sliding contact between hard microasperities on the particle surface and the softer aluminum. Sharp, irregular particles (lighter contrast, Fig. 11b) were found attached to a vertical section of the wall. The average Cu:Al at.% ratio was 1.0 ± 0.3. Despite the fine probe size used for EDX analysis, the small size of the particles did not preclude some contribution from the substrate underneath. Nevertheless, it was clear that they contained a significant concentration of copper. It is proposed that they were sheared-off pieces of material from the particle that had adhered to the substrate.

The cratered 7050 surface showed dimpling, and fine, protruding nodules (Fig. 12). EDX analysis produced a

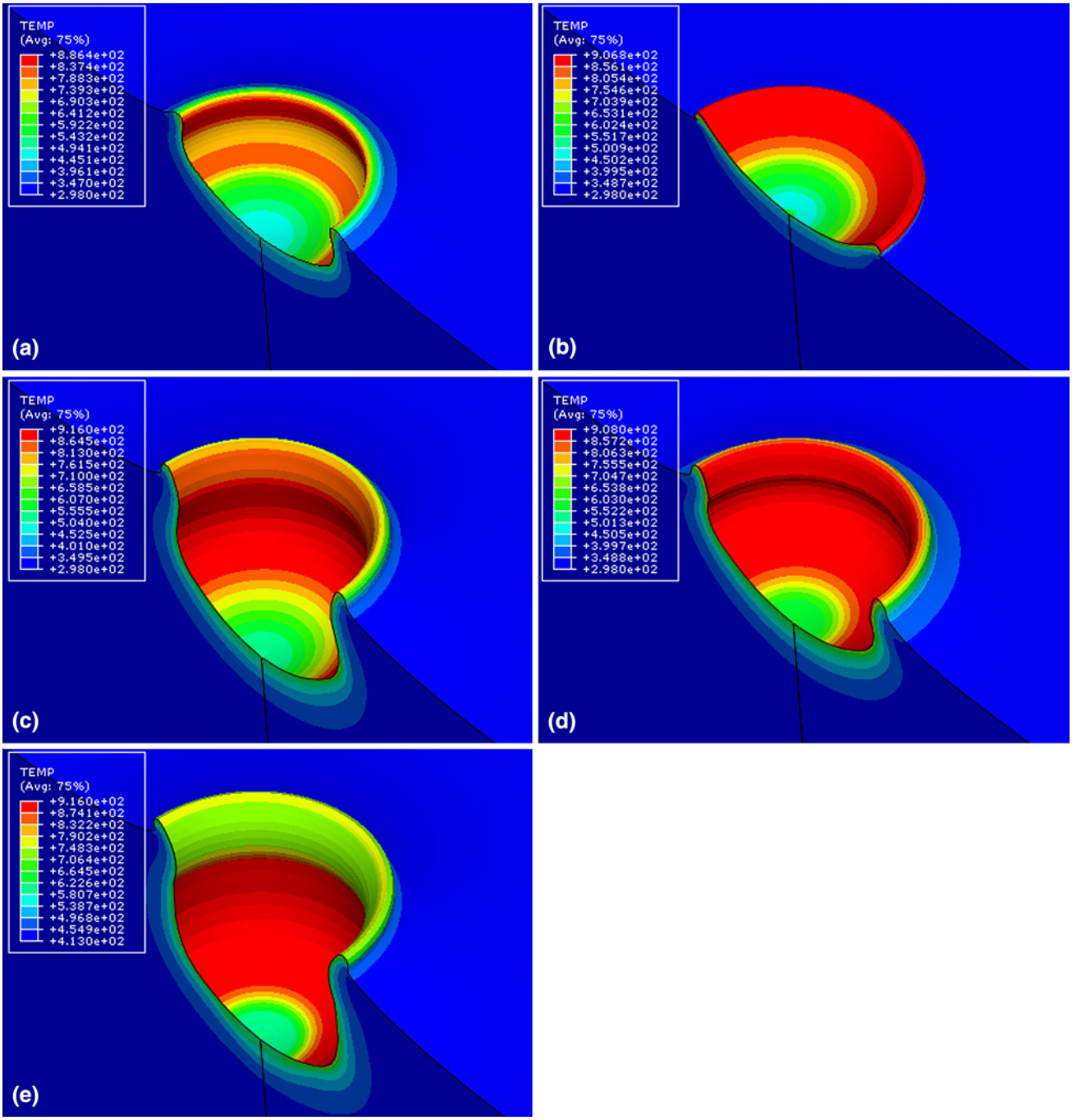

Fig. 8 Substrate-side distribution of interfacial temperature; (a) Cu-Al1100, $v_i = 430$ m/s, (b) Cu-Al7075, $v_i = 430$ m/s, (c) Cu-Al1100, $v_i = 670$ m/s, (d) Cu-Al7075, $v_i = 670$ m/s, and (e) Cu-Al1100, $v_i = 670$ m/s, substrate $T_i = 413$ K

mixed result. Smooth, spherical, or vaguely spherical nodules tended to be high in aluminum (e.g., Point *A* in Fig. 12, Cu:Al at.% ratio = 0.20). *B* (Cu:Al at.% ratio = 0.06) is a feature that appears to have spread across the surface. However, irregular, lumpy particles, were mainly copper-based (*C* Cu:Al at.% ratio = 2.0). Note that at low-impact velocities, FE modeling predicted higher interfacial temperatures on the harder alloy surface compared with the softer one, which seems consistent with the increased signs of melt formation here.

Modeling predicted that the effect of increasing impact velocity would be stronger strain localization within the substrate and larger areas of the interface (from the substrate side) reaching melting point. Observation of impact sites on the softer substrate with T_0 increased to 600 °C found lips that protruded from the rims of the craters, and

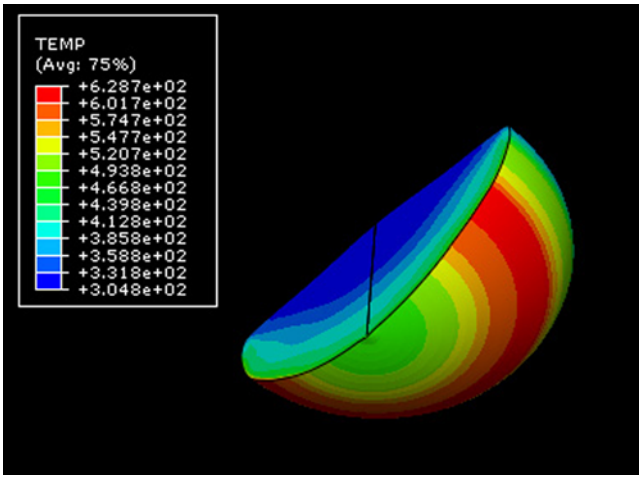

Fig. 9 Particle-side distribution of interfacial temperatures, Cu-Al1100, $v_i = 670$ m/s

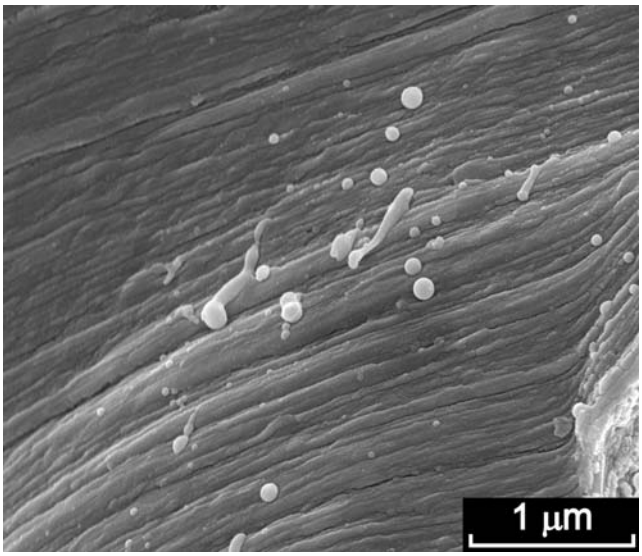

Fig. 10 Splashes of aluminum (ejecta) outside a crater at $T_0 = 200$ °C

which were not present at 200 °C. These lips were even more pronounced on the 7050 substrate (Fig. 6b).

On exposed sections of the crater walls on CP Al at 600 °C, pronounced vertical scratches were due to sliding of the rough particle surface over the aluminum (Fig. 13). Horizontal cracks may have been the result of contraction on cooling of an outer, heated layer. Lumpy areas (marked by arrow, Fig. 13) may too have formed by the same process. The ''bare'' sections of the wall contained little or no Cu (Cu:Al at.% ratio <0.05). Attached particles could be categorized as either smooth and spherical (Cu:Al at.% $= 0.10 \pm 0.04$), or irregular (Cu:Al at.% $= 2.6 \pm 1.0$).

On the 7050 substrate, particles attached to the interior wall (inset in Fig. 6b) had mainly an irregular appearance.

3.5 TEM Interfacial Study (Cu-on-CP Al, $T_0 = 600$ °C only)

One sample (the Cu-on-CP Al, $T_0 = 600$ °C) was chosen for more detailed analysis of the bonded interface. No real difference could be discerned between the base of the

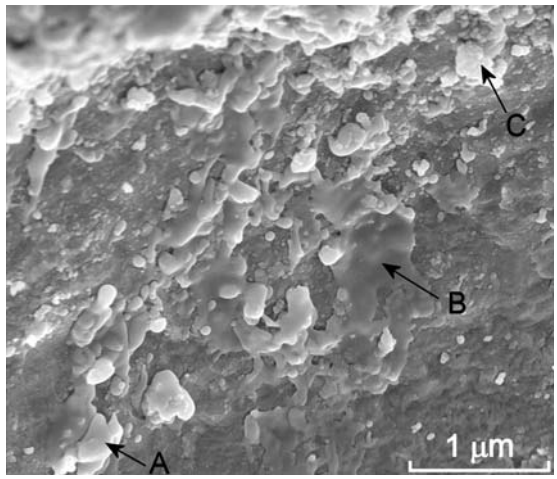

Fig. 12 Empty crater surface following impact onto Al7050 at $T_0 = 200$ °C

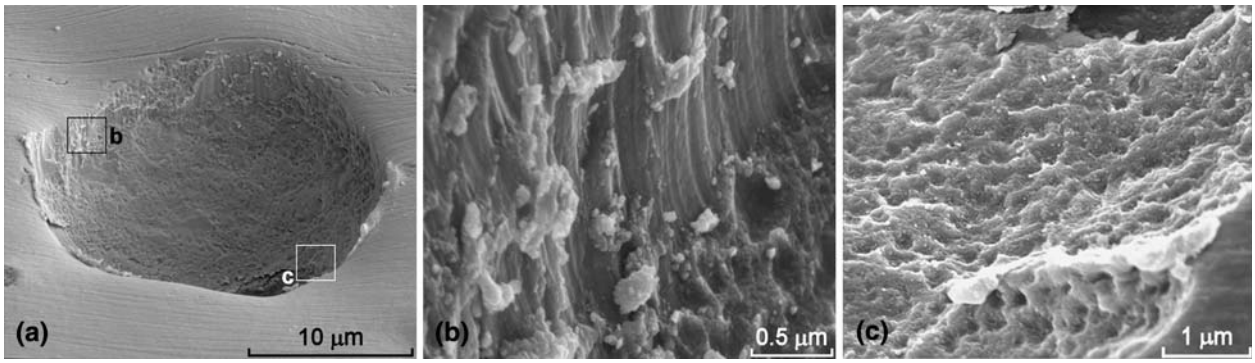

Fig. 11 (a) SE image of an empty crater on the CP Al surface following $T_0 = 200$ °C impact. (b, c) Higher magnification images of parts of the crater

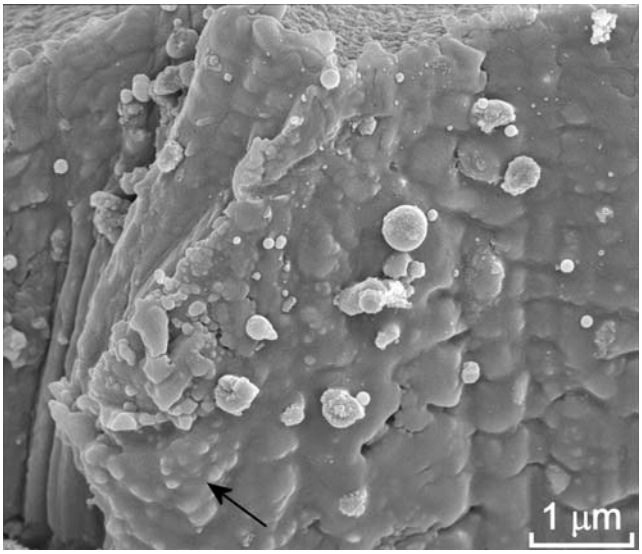

Fig. 13 Vertical crater wall on CP Al, $T_0 = 600$ °C

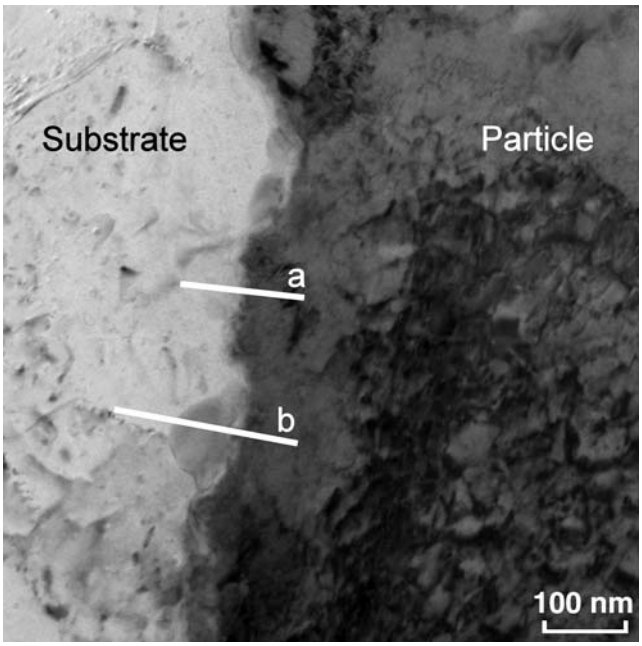

Fig. 14 Bright field image of Cu-CP Al interface. EDX scans over lines (a) and (b) are shown in Fig. 15

particle and the periphery. Figure 14 is a representative micrograph. Reaction between the particle and substrate had occurred intermittently along the interface. EDX line traces were made at several places (Fig. 15). In some places the particle/substrate boundary was abrupt (a). In others there was an intermetallic zone (b) up to ~50 nm in thickness, whose composition was close to that of stoichiometric $CuAl_2$ (54.1 wt.%Cu:45.9 wt.% Al). The $CuAl_2$/Cu interface was very sharp, while the Al/$CuAl_2$ interface was less so, which may have indicated a limited

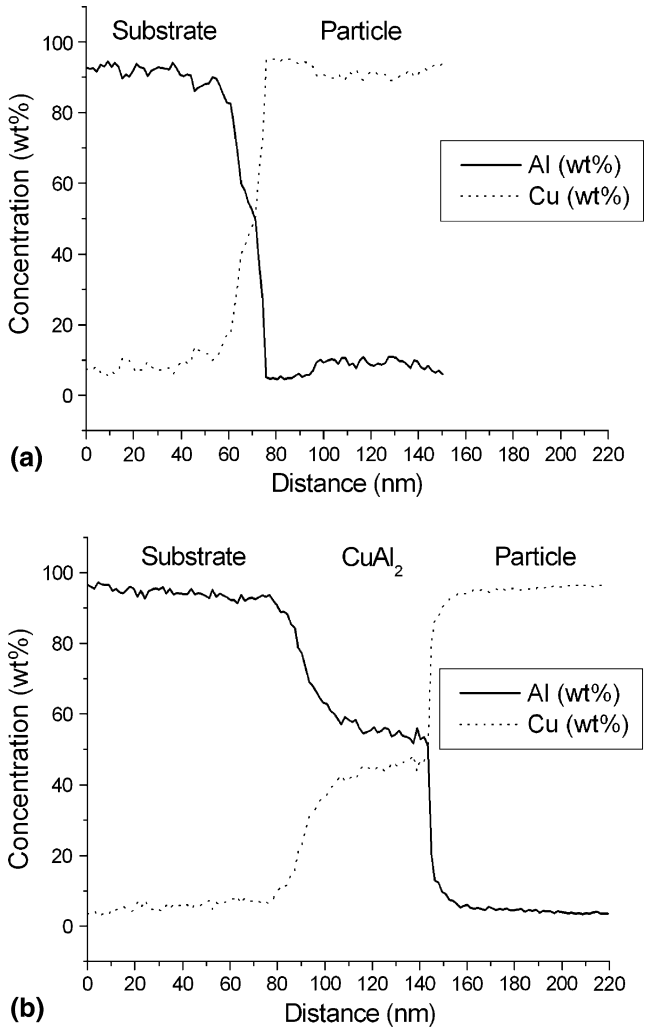

Fig. 15 EDX line scans at the positions indicated in Fig. 14

amount of diffusion of copper beyond the intermetallic zone into the aluminum. A selected area diffraction pattern (SADP) taken from an area of the interface identified two neighboring grains of $CuAl_2$ (Fig. 16). While the Cu-Al phase diagram contains a number of other intermetallics, none of them were detected in this sample.

4. Discussion

It was clear, from the computer simulations and SEM observations, that a certain amount of substrate material had reached melting point, generating splashes of material inside the craters and outside (ejecta), without much mixing with copper from the particles. At the very least, formation of a liquid film may have aided in wetting the particle surface and increasing the surface-to-surface contact area. However, a great improvement in adhesion could be expected if melting were to facilitate atomic mixing at the interface. Copper itself melts at 1356 K, which was not achievable by deformation against the

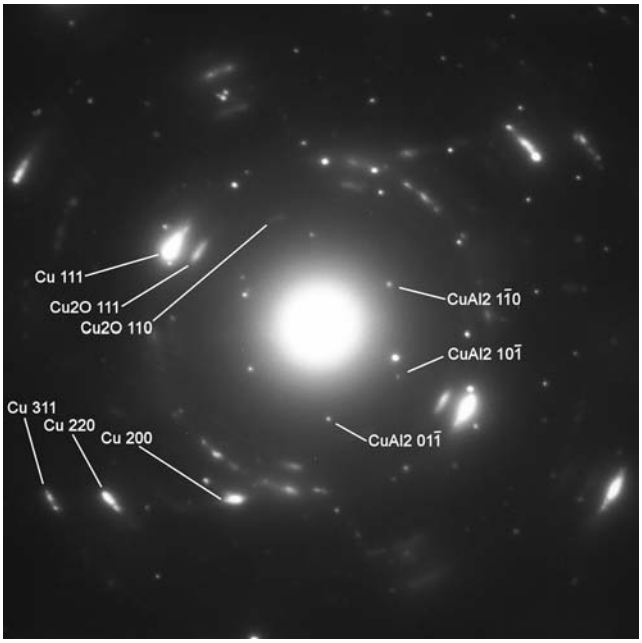

Fig. 16 Selected area diffraction pattern of the Cu-CP Al interface, showing two sets of $CuAl_2$ diffraction spots

softer substrate materials at these velocities. However, this does not exclude the possibility of formation of a low-melting point phase upon contact with the aluminum, provided that atomic inter-diffusion occurred within a liquid eutectic layer. The Al-$CuAl_2$ eutectic is at 812 K.

A similar line of argument to that used in earlier studies (Ref 19) can now be taken to show that the existence of an intermetallic necessitates the presence of liquid. The diffusivity of copper in solid solution in aluminum at 812 K is 1.1×10^{-13} m^2/s (Ref 45). Within a maximum 48 ns contact time, the diffusion distance $\sqrt{Dt}$ is only 0.07 nm. This is even less than the lattice parameter of aluminum, 0.4 nm. Therefore, diffusion in the solid state can be, for all practical purposes, ignored. In contrast, the diffusivity of Cu in liquid aluminum has been measured at 4.2×10^{-9} m^2/s—four orders of magnitude higher than in the solid—using a pulsed laser technique which eliminates convection (Ref 46). This yields $\sqrt{Dt} = 14$ nm as a lower estimate, but it is likely that if the effects of convection and turbulent mixing in the liquid film were included, that would permit transport of copper over even larger distances.

A melting point layer thickness of 85 nm was predicted by FEM in the 670 m/s impact of Cu onto Al 1100 at 413 K. As previously mentioned, the numerical code did not include the effect of heat conduction. Since it did not allow for heat transfer away from the interface toward the particle and substrate interiors during deformation, it has been suggested that this may lead to interfacial temperatures being overestimated (Ref 47). In comparison, at the location chosen for TEM study, it was seen that some $CuAl_2$ grains had grown to 50 nm thickness, and some further 20-30 nm of copper diffusion into aluminum may have occurred. In the FIB/SEM, the interfacial phase was observed over 80 nm thick. Thus, close agreement was found between modeling and experiment.

Microroughness on the particle surface may have been another contributing factor to heating of the substrate surface. Deep scratching during sliding of hard particle asperities over the softer aluminum, may have promoted local melting due to stress concentration at these points. Copper-containing debris found in the craters was material that had broken off from the tips of these asperities and adhered to the substrate by interaction with the molten layer.

It was seen that interfacial melting occurred even at the lowest stagnation temperature, for which substrate heating was minimal, and indeed, modeling at room temperature showed that the melting point could be reached solely by heat evolved from adiabatic shearing. However, at $T_0 = 600$ K, the large amount of melting at the base of the particle as well as the periphery, more closely resembled the simulation with the preheated substrate. In Section 3.3 too, a better match was found for penetration depth between simulation and experiment if the simulation included a heated substrate (Fig. 7a). Both facts suggest that at high T_0, the bow shock interaction between the gas jet and the substrate, which results in heating of the surface, does play an important role in bonding. Similarly, other researchers have found improved bonding by heating the substrate (Ref 48, 49).

In comparison with other studies, the intermetallic formation was rather limited. Barradas et al. (Ref 19) and Guetta et al. (Ref 8), who cold-sprayed copper particles onto aluminum substrates under similar conditions, describe a thicker intermetallic zone, containing a wide range of phases. Differences in feedstock material may be the main cause, since both impurities and the powder manufacturing route may influence the properties of the surface oxide layer present. It has been shown (Ref 50) that the thickness of the oxide layer may have a large bearing on bonding behavior. A thick oxide layer may present a barrier to intermetallic formation.

While it was clearly demonstrated that melting is present in penetrative copper-onto-aluminum impact, it is still difficult to draw more general conclusions on its effect on bonding without the availability of similar, detailed studies into other cold spray systems. Cold spray bonding is often compared with explosive welding. In that process, it is known that jetting aids in the removal of surface contaminants and the formation of a strong bond between the colliding plates. In addition to jetting, under certain conditions bonding occurs together with interfacial melting, while in other cases, bonding takes place in the absence of melting (Ref 51, 52). At this stage, there is insufficient information to make an analogous statement about cold spray. Furthermore, adhesion of individual particles must surely be influenced by the condition of the interface at the moment that elastic rebound occurs, which given the small size of the particles, is not long after initial contact. However, it is not known how long the interfacial layer remained molten without a combined heat conduction/deformation model, which was not attempted here.

5. Conclusions

A variety of copper particle impact conditions onto aluminum during cold spray deposition have been investigated. A more localized deformation characteristic and higher interfacial temperatures were produced on the aerospace alloy 7050, compared with the soft, CP aluminum. At low velocities on the harder substrate, deformation was more evenly shared between particle and substrate. The penetrative regime was reached at higher velocities on 7050, and under all conditions on the CP grade. Penetration depth increased with v_i. Jetting in the particle was suppressed due to much greater absorption of impact energy by substrate deformation. Trapping of the particles physically within the craters may have contributed to the higher deposition efficiencies observable at high velocities, particularly on the CP substrate.

According to the FE model, the temperature rise in the wall of the crater due to adiabatic shearing reached melting point for velocities 430 m/s and greater, encompassing a greater fraction of the interface with increasing v_i. Melting was confirmed experimentally. The duration and extent of melting were sufficiently large to cause the intermetallic phase $CuAl_2$ to form. This could not be explained without allowing for diffusion within a eutectic melt.

At the highest stagnation temperature, heat transfer from the gas phase, which could raise the surface temperature to a maximum of 413 K in one pass, increased both particle penetration and melting.

Acknowledgments

This work was supported by a Korean Science and Engineering Foundation (KOSEF) grant funded by the Korean government (MOST) (No. 2006-02289). The authors would like to thank Jens Oqueka, from Helmut Schmidt University, University of the Federal Armed Forces, Hamburg, Germany, for his assistance in implementing some of the particle acceleration model into code.

References

1. A. Papyrin, V. Kosarev, S. Klinkov, A. Alhimov, and V. Fomin, *Cold Spray Technology*, Elsevier, Amsterdam, 2007
2. R.C. McCune, A.N. Papyrin, J.N. Hall, W.L. Riggs, and P.H. Zajchowski, An Exploration of the Cold Gas-Dynamic Spray Method for Several Materials Systems, *Proceedings, 8th National Thermal Spray Conference*, C.C. Berndt and S. Sampath, Eds., ASM International, Materials Park, OH, 1995, p 1-5
3. P.C. King, S.H. Zahiri, M. Jahedi, and J. Friend, Cold Spray Electroding of Piezoelectric Ceramic, *Mater. Forum*, 2007, **31**, p 116-119
4. P.C. King, S.H. Zahiri, and M.Z. Jahedi, Rare Earth/Metal Composite Formation by Cold Spray, *J. Therm. Spray Technol.*, 2007, **17**(2), p 221-227
5. T. Stoltenhoff, H. Kreye, and H.J. Richter, An Analysis of the Cold Spray Process and Its Coatings, *J. Therm. Spray Technol.*, 2002, **11**(4), p 542-550
6. M. Grujicic, C.L. Zhao, W.S. DeRosset, and D. Helfritch, Adiabatic Shear Instability Based Mechanism for Particles/Substrate Bonding in the Cold-Gas Dynamic-Spray Process, *Mater. Design*, 2004, **25**(8), p 681-688
7. P.C. King, S.H. Zahiri, and M.H. Jahedi, Focussed Ion Beam Micro-Dissection of Cold Sprayed Particles, *Acta Mater.*, 2008, **56**(19), p 5617-5626
8. S. Guetta, M.H. Berger, F. Borit, V. Guipont, M. Jeandin, M. Boustie, F. Poitiers, Y. Ichikawa, and K. Ogawa, Influence of Particle Velocity on Adhesion of Cold-Sprayed Splats, *Thermal Spray 2008: Crossing Borders*, E. Lugscheider, Ed., ASM International, Materials Park, OH, 2008,
9. P.C. King, S.H. Zahiri, and M. Jahedi, Microstructural Refinement Within a Cold Sprayed Copper Particle, *Metall. Mater. Trans. A*, 2009, **40**(9), p 2115-2123
10. H. Assadi, F. Gartner, T. Stoltenhoff, and H. Kreye, Bonding Mechanism in Cold Gas Spraying, *Acta Mater.*, 2003, **51**(15), p 4379-4394
11. G. Bae, Y. Xiong, S. Kumar, K. Kang, and C. Lee, General Aspects of Interface Bonding in Kinetic Sprayed Coatings, *Acta Mater.*, 2008, **56**(17), p 4858-4868
12. M. Grujicic, J.R. Saylor, D.E. Beasley, W.S. DeRosset, and D. Helfritch, Computational Analysis of the Interfacial Bonding Between Feed-Powder Particles and the Substrate in the Cold-Gas Dynamic-Spray Process, *Appl. Surf. Sci.*, 2003, **219**(3-4), p 211-227
13. R.C. Dykhuizen, M.F. Smith, D.L. Gilmore, R.A. Neiser, X. Jiang, and S. Sampath, Impact of High Velocity Cold Spray Particles, *J. Therm. Spray Technol.*, 1999, **8**(4), p 559-564
14. A.P. Alkhimov, S.V. Klinkov, and V.F. Kosarev, Temperature Near the Contact Boundary at High-Velocity Collision of a Microparticle and a Surface, *Phys. Mesomech.*, 2000, **3**, p 53-57
15. X.-J. Ning, J.-H. Jang, H.-J. Kim, C.-J. Li, and C. Lee, Cold Spraying of Al-Sn Binary Alloy: Coating Characteristics and Particle Bonding Features, *Surf. Coat. Technol.*, 2008, **202**, p 1681-1687
16. C.-J. Li, W.-Y. Li, and Y.-Y. Wang, Formation of Metastable Phases in Cold-Sprayed Soft Metallic Deposit, *Surf. Coat. Technol.*, 2005, **198**(1-3), p 469-473
17. J. Wu, H. Fang, H. Kim, and C. Lee, High Speed Impact Behaviors of Al Alloy Particle onto Mild Steel Substrate During Kinetic Deposition, *Mater. Sci. Eng. A*, 2006, **417**(1-2), p 114-119
18. W.-Y. Li, C. Zhang, X. Guo, C.-J. Li, H. Liao, and C. Coddet, Study on Impact Fusion at Particle Interfaces and Its Effect on Coating Microstructure in Cold Spraying, *Appl. Surf. Sci.*, 2007, **254**(2), p 517-526
19. S. Barradas, V. Guipont, R. Molins, M. Jeandin, M. Arrigoni, M. Boustie, C. Bolis, L. Berthe, and M. Ducos, Laser Shock Flier Impact Simulation of Particle-Substrate Interactions in Cold Spray, *J. Therm. Spray Technol.*, 2007, **16**(4), p 475-479
20. S. Guetta, M. Berger, F. Borit, V. Guipont, M. Jeandin, M. Boustie, Y. Ichikawa, K. Sakaguchi, and K. Ogawa, Influence of Particle Velocity on Adhesion of Cold-Sprayed Splats, *J. Therm. Spray Technol.*, 2009, **18**(3), p 331–342
21. A. Wank, B. Wielage, H. Podlesak, and T. Grund, High-resolution microstructural investigations of interfaces between light metal alloy substrates and cold gas-sprayed coatings, *J. Therm. Spray Technol.*, 2006, **15**(2), p 280-283
22. A.V. Bolesta, V.M. Fomin, M.R. Sharafutdinov, and B.P. Tolochko, Investigation of Interface Boundary Occurring During Cold Gas-Dynamic Spraying of Metallic Particles, *Nucl. Instrum. Meth. A*, 2001, **470**(1-2), p 249-252
23. J.L. Robinson, Fluid Mechanics of Copper: Viscous Energy Dissipation in Impact Welding, *J. Appl. Phys.*, 1977, **48**(6), p 2202-2207
24. V.K. Champagne, D. Helfritch, P. Leyman, S. Grendahl, and B. Klotz, Interface Material Mixing Formed by the Deposition of Copper on Aluminium by Means of the Cold Spray Process, *J. Therm. Spray Technol.*, 2005, **14**(3), p 330-334
25. K. Balani, A. Agarwal, S. Seal, and J. Karthikeyan, Transmission Electron Microscopy of Cold Sprayed 1100 Aluminum Coating, *Scripta Mater.*, 2005, **53**(7), p 845-850
26. Y. Xiong, K. Kang, G. Bae, S. Yoon, and C. Lee, Dynamic Amorphization and Recrystallization of Metals in Kinetic Spray Process, *Appl. Phys. Lett.*, 2008, **92**, p 194101

27. K. Kim, M. Watanabe, K. Mitsuishi, K. Iakoubovskii, and S. Kuroda, Impact Bonding and Rebounding Between Kinetically Sprayed Titanium Particle and Steel Substrate Revealed by High-Resolution Electron Microscopy, *J. Phys. D Appl. Phys.*, 2009, **42**(6), p 5
28. R.C. Dykhuizen and M.F. Smith, Gas Dynamic Principles of Cold Spray, *J. Therm. Spray Technol.*, 1998, **7**(2), p 205-212
29. W.Y. Li and C.J. Li, Optimal Design of a Novel Cold Spray Gun Nozzle at a Limited Space, *J. Therm. Spray Technol.*, 2005, **14**(3), p 391-396
30. B. Jodoin, Cold Spray Nozzle Mach Number Limitation, *J. Therm. Spray Technol.*, 2002, **11**(4), p 496-507
31. S.P. Pardhasaradhi, V. Venkatachalapathy, S.V. Joshi, and S. Govindan, Optical Diagnostics Study of Gas Particle Transport Phenomena in Cold Gas Dynamic Spraying and Comparison with Model Predictions, *J. Therm. Spray Technol.*, 2008, **17**(4), p 551-563
32. J.D. Anderson, *Modern Compressible Flow: with Historical Perspective*, 3rd ed., McGraw-Hill, New York, 2003
33. Fluent 6.1 User's Guide, ANSYS, Inc., Canonsburg, PA
34. C.B. Henderson, Drag Coefficients of Spheres in Continuum and Rarefied Flows, *AIAA J.*, 1976, **14**(6), p 707-708
35. D.L. Gilmore, R.C. Dykhuizen, R.A. Neiser, T.J. Roemer, and M.F. Smith, Particle Velocity and Deposition Efficiency in the Cold Spray Process, *J. Therm. Spray Technol.*, 1999, **8**(4), p 576-582
36. L.A. Giannuzzi and F.A. Stevie, A Review of Focused Ion Beam Milling Techniques for TEM Specimen Preparation, *Micron*, 1999, **30**(3), p 197-204
37. J. Li, T. Malis, and S. Dionne, Recent Advances in FIB-TEM Specimen Preparation Techniques, *Mater. Charact.*, 2006, **57**(1), p 64-70
38. ABAQUS™ 6.7-2 User Manual, Dessault Systemes Simulia Corp., Providence, RI, 2007
39. G.R. Johnson, and W.H. Cook, A Constitutive Model and Data for Metals Subjected to Large Strains, High Strain Rates and High Temperatures, *Proceedings of the 7th International Ballistics Symposium*, 1983, p 541-547
40. Matweb, Available from: www.matweb.com
41. K.A. Dannemann, C.E. Anderson, and G.R. Johnson, Modeling the Ballistic Impact Performance of Two Aluminum Alloys, *Modelling the Performance of Engineering Structural Materials II*, D.R. Leseur and T.S. Srivatsan, Ed., TMS, 2001, p 63-74
42. W. Herrmann and J.S. Wilbeck, Review of Hypervelocity Penetration Theories: Hypervelocity Impact Proceedings of the 1986 Symposium, *Int. J. Impact Eng.*, 1987, **5**(1-4), p 307-322
43. L.E. Murr, S.A. Quinones, E. Ferreyra, T.A. Ayala, O.L. Valerio, F. Horz, and R.P. Bernhard, The Low-Velocity-to-Hypervelocity Penetration Transition for Impact Craters in Metal Targets, *Mater. Sci. Eng. A*, 1998, **256**(1-2), p 166-182
44. E. Irissou, J.G. Legoux, C. Moreau, and A.N. Ryabinin, How Cold is Cold Spray? An Experimental Study of the Heat Transfer to the Substrate in Cold Gas Dynamic Spraying, *Thermal Spray 2008: Crossing Borders*, E. Lugscheider, Ed., ASM International, Materials Park, OH, 2008
45. M.S. Anand, S.P. Murarka, and R.P. Agarwala, Diffusion of Copper in Nickel and Aluminum, *J. Appl. Phys.*, 1965, **36**(12), p 3860-3862
46. N. Isono, P. Smith, D. Turnbull, and M. Aziz, Anomalous Diffusion of Fe in Liquid Al Measured by the Pulsed Laser Technique, *Metall. Mater. Trans. A*, 1996, **27**(3), p 725-730
47. K. Yokoyama, M. Watanabe, S. Kuroda, Y. Gotoh, T. Schmidt, and F. Gartner, Simulation of Solid Particle Impact Behavior for Spray Processes, *Mater. Trans.*, 2006, **47**(7), p 1697-1702
48. J. Legoux, E. Irissou, and C. Moreau, Effect of Substrate Temperature on the Formation Mechanism of Cold-Sprayed Aluminum, Zinc and Tin Coatings, *J. Therm. Spray Technol.*, 2007, **16**(5), p 619-626
49. M. Fukumoto, H. Wada, K. Tanabe, M. Yamada, E. Yamaguchi, A. Niwa, M. Sugimoto, and M. Izawa, Effect of Substrate Temperature on Deposition Behavior of Copper Particles on Substrate Surfaces in the Cold Spray Process, *J. Therm. Spray Technol.*, 2007, **16**(5), p 643-650
50. K. Kang, S. Yoon, Y. Ji, and C. Lee, Oxidation Dependency of Critical Velocity for Aluminum Feedstock Deposition in Kinetic Spraying Process, *Mater. Sci. Eng. A*, 2008, **486**(1-2), p 300-307
51. G.R. Cowan and A.H. Holtzman, Flow Configurations in Colliding Plates: Explosive Bonding, *J. Appl. Phys.*, 1963, **34**(4), p 928-939
52. B. Crossland and J.D. Williams, Explosive Welding, *Met. Mater.*, 1970, **4**, p 79-100
53. J. Vlcek, L. Gimeno, H. Huber, and E. Lugscheider, A Systematic Approach to Material Eligibility for the Cold-Spray Process, *J. Therm. Spray Technol.*, 2005, **14**(1), p 125-133
54. D. Zhang, P.H. Shipway, and D.G. McCartney, Cold Gas Dynamic Spraying of Aluminium: The Role of Substrate Characteristics in Deposit Formation, *J. Therm. Spray Technol.*, 2005, **14**(1), p 109-116